Reactions of the *B*-Phenylborole Complex [CpRh(η^5-C_4H_4BPh)] with Metalloelectrophiles [(ring)M]$^{2+}$

Dmitry A. Loginov,[a] Dmitry V. Muratov,[a] Pavel V. Petrovskii,[a] Zoya A. Starikova,[a] Maddalena Corsini,[b] Franco Laschi,[b] Fabrizia de Biani Fabrizi,[b] Piero Zanello,[b] and Alexander R. Kudinov*[a]

Keywords: Boron / Electrochemistry / Heterocycles / Rhodium / Sandwich compounds

Thirty-valence-electron dicationic triple-decker complexes with a bridging borole ligand [CpRh(μ-η^5:η^5-C_4H_4BPh)M(ring)]$^{2+}$ [M(ring) = CoCp* (**3**), IrCp* (**6**), Ru(η-$C_6H_3Me_3$-1,3,5) (**8a**), Ru(η-C_6Me_6) (**8b**)] were obtained by stacking reactions of [CpRh(η^5-C_4H_4BPh)] (**2**) with the corresponding half-sandwich fragments [M(ring)]$^{2+}$. Minor formation of arene-type complexes [CpRh(μ-η^5:η^6-C_4H_4BPh)M(ring)]$^{2+}$ was observed for M(ring) = IrCp* and Ru(arene). On the contrary, the arene-type complex [CpRh(μ-η^5:η^6-C_4H_4BPh)RhCp*]$^{2+}$ (**5**) was isolated as the sole product from the reaction of **2** with the fragment [RhCp*]$^{2+}$; an intermediate formation of the triple-decker complex [CpRh(μ-η^5:η^5-C_4H_4BPh)RhCp*]$^{2+}$ (**4**) in this reaction was detected by ^{1}H NMR spectroscopy. Heating **6** in nitromethane gives the symmetrical triple-decker complex [Cp*Ir(μ-η^5:η^5-C_4H_4BPh)IrCp*]$^{2+}$ (**10**). The cations were isolated as salts with the BF_4^- anion. The structures of **2**, **5**$(BF_4)_2$, **6**$(BF_4)_2$ and **8a**$(BF_4)_2$ were determined by X-ray diffraction. The electrochemical properties of the complexes were also investigated.

Introduction

The interaction of arenes with 12-valence-electron (VE) metal complex fragments affords arene complexes. For instance, by using dicationic fragments [(ring)M]$^{2+}$ [(ring)M = Cp*Rh, Cp*Ir, (arene)Ru] in the form of their labile solvates with acetone, a great number of arene complexes [(ring)M(arene)]$^{2+}$ has been prepared.[1] A closely related reaction − the electrophilic stacking of sandwich compounds with [(ring)M]$^{n+}$ (n = 1, 2) fragments − has proved to be an effective method for the synthesis of cationic triple-decker complexes.[2] In particular, using this method, complexes with bridging five-electron ligands (cyclopentadienyl[3] and boratabenzene[4]) have been obtained. Herberich et al.[5] have prepared 30 VE triple-decker complexes [(ring)M(μ-η^5:η^5-C_4H_4BPh)CoCp]$^{2+}$ [(ring)M = Cp*Ir and (C_6Me_6)Ru] with a central four-electron borole ligand by reaction of the fragments [(ring)M]$^{2+}$ with the (*B*-phenylborole)cobalt complex [CpCo(η^5-C_4H_4BPh)] (**1**). In a similar reaction with the cyclohexyl-substituted analogue [CpCo(η^5-C_4H_4BCy)] we have synthesized the complexes [(ring)M(μ-η^5:η^5-C_4H_4BCy)CoCp]$^{2+}$ [(ring)M = Cp*Rh, (C_6H_6)Ru, (1,3,5-$C_6H_3Me_3$)Ru; Cy = cyclohexyl].[6]

[a] A. N. Nesmeyanov Institute of Organoelement Compounds, 28 ul. Vavilova, 119991 Moscow, GSP-1, Russian Federation
Fax: +7-095-135-5085
E-mail: arkudinov@ineos.ac.ru
[b] Dipartimento di Chimica, Universitá di Siena, Via Aldo Moro, 53100 Siena, Italy

It is noteworthy that in the case of the phenyl-substituted complexes **1** and [CpRh(η^5-C_4H_4BPh)] (**2**) there are two possible places for attack by the metalloelectrophile: the borole ring or the phenyl substituent. However, for the cobalt complex **1** only electrophilic attack at the borole ligand has been described.[5] Herein we report the reactions of the analogous rhodium complex **2** with dicationic fragments [(ring)M]$^{2+}$ as well as the results of structural and electrochemical study of the products.

Results and Discussion

Stacking Reactions

The electrophilic stacking reaction of **2** with the dicationic fragment [Cp*Co]$^{2+}$ (in the form of its nitromethane solvate)[7] yields the 30 VE triple-decker complex **3** as the sole product, which suggests that the electrophilic attack proceeds exclusively at the borole ring (Scheme 1).[8] The absence of a product formed by attack at the phenyl substituent is in accordance with the known fact that the fragment [Cp*Co]$^{2+}$ does not react with benzene under such conditions.[9]

On the contrary, in the case of a similar reaction with the [Cp*Rh]$^{2+}$ fragment (in the form of its nitromethane or acetone solvate) only the arene-type complex **5** was isolated (Scheme 2). However, it was shown by means of ^{1}H NMR spectroscopy that the starting materials disappear within 5 min in [D_3]nitromethane and the mixture formed contains

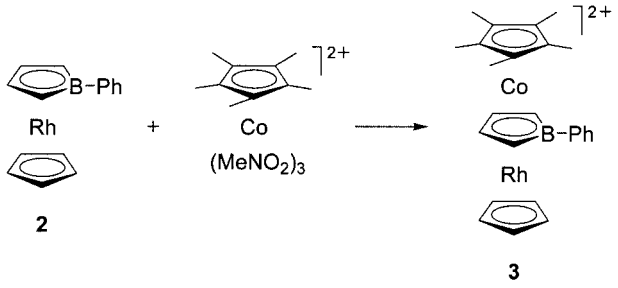

Scheme 1. Formation of the triple-decker complex **3**.

both complex **5** and the triple-decker complex **4** in a ratio of about 1:9. After 4 h the signals of **4** disappear and the intensities of the signals of **5** increase, thus suggesting that **4** is unstable at room temperature and transforms into the arene-type complex **5**. It may be concluded that the initial attack of $[Cp^*Rh]^{2+}$ proceeds at the borole ring with its subsequent transfer to the benzene ring.

The stacking reaction of **2** with the iridium-containing fragment $[Cp^*Ir]^{2+}$, as its $MeNO_2$ solvate, affords the RhIr triple-decker complex **6** which, according to ^1H NMR spectroscopy, contains an admixture of the arene-type complex **7** (ca. 6%) (Scheme 3). In contrast to **4**, both **6** and **7** are stable at room temperature and do not interconvert. Unfortunately, we were unable to purify **6** either by recrystallization or by chromatography. Nevertheless, the content of **7** in the product can be decreased to about 4% by lowing the reaction temperature to –15 °C; this suggests that the electrophilic attack is kinetically controlled. The use of acetone instead of $MeNO_2$ leads to a further decrease of the admixture content (0.8%), apparently due to a slowing of the process caused by the lower reactivity of the acetone solvate. The best purity achieved for the triple-decker **6** was more than 99%. In a similar manner, the reaction of **2** with $[(arene)Ru]^{2+}$ fragments (arene = 1,3,5-$C_6H_3Me_3$, C_6Me_6) yields the RhRu triple-decker complexes **8a**,**b** contaminated with the arene-type complexes **9a**,**b**. The best purity of **8a**,**b** (achieved using acetone as a solvent at –15 °C) was about 97%.

We studied the thermal transformation of the triple-decker complexes **6** and **8a**,**b**, and found that the RhIr complex **6** transforms into the diiridium analogue **10** in refluxing nitromethane, apparently as a result of a symmetrization reaction (Scheme 4);[10] the absence of the corresponding dirhodium complex $[CpRh(\mu\text{-}\eta^5\text{:}\eta^5\text{-}C_4H_4BPh)RhCp]^{2+}$ may be explained by its low stability. However, the reaction is rather slow (according to ^1H NMR spectroscopy the degree of conversion is about 30% after 12 h) and we were unable to obtain complex **10** in pure form. Obviously,

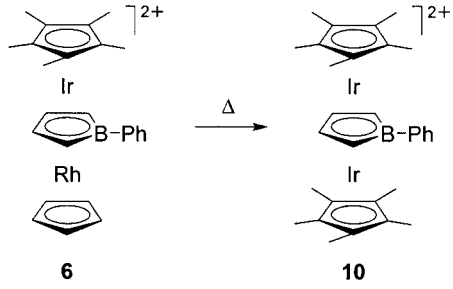

Scheme 4. Thermal transformation of complex **6**.

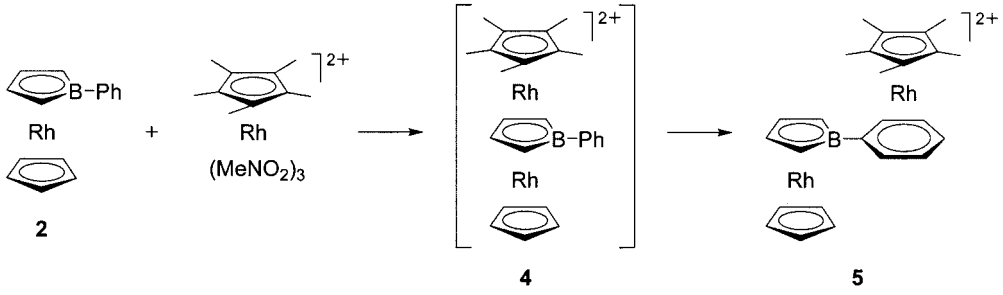

Scheme 2. Formation of the arene-type complex **5**.

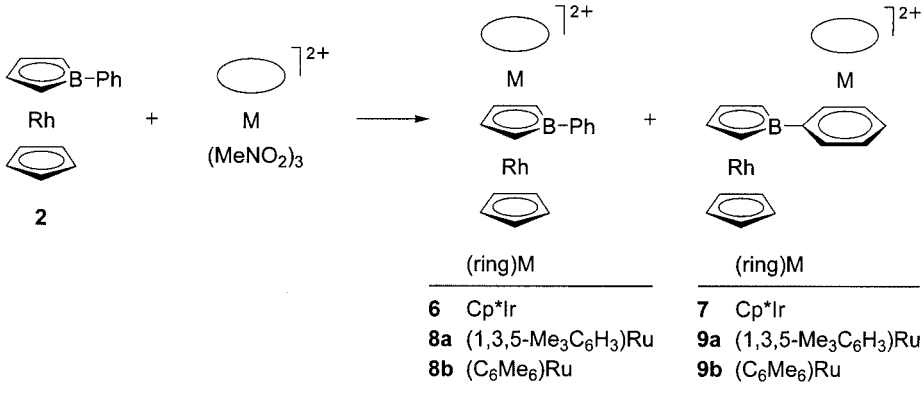

Scheme 3. Reactions of **2** with the fragments $[Cp^*Ir]^{2+}$ and $[(arene)Ru]^{2+}$.

Table 1. ^1H and ^{11}B NMR spectroscopic data for complexes **2**[21] and **3**–**10**.[a]

	^1H NMR					^{11}B NMR	
	2-/5-H[b]	3-/4-H[b]	RhCp[c]	ML[c]	Ph[b]	C_4H_4B[d]	BF_4^- [c]
2	4.43[e]	5.28[e]	5.17[e]		7.64 (H_o), 7.24 (H_m, H_p)[e]	16.8[f]	
3[g]	5.46	6.57	6.16	1.85 (Cp*)	7.95 (H_o), 7.53 (H_m, H_p)	14.0	–0.1
4[h][i]	5.30	6.24	6.12	1.83 (Cp*)	7.71 (H_o), 7.46 (H_m, H_p)	[j]	[j]
5[g]	4.83	5.62	5.48	2.20 (Cp*)	7.60 (H_o), 7.42 (H_m, H_p)	10.2	–0.2
6[g]	5.55	6.48	6.44	1.97 (Cp*)	7.78 (H_o), 7.46 (H_m), 7.37 (H_p)	10.2	–0.2
7[g][i]	4.79	5.60	5.50	2.32 (Cp*)	[k]	[k]	[k]
8a[g]	5.44	6.43	6.35	6.36 ($C_6H_3Me_3$) 2.21 ($C_6H_3Me_3$)	7.84 (H_o), 7.42 (H_m, H_p)	13.7	–0.1
8b[g]	5.29	6.30	6.24	2.26 (C_6Me_6)	7.78 (H_o), 7.49 (H_m), 7.43 (H_p)	13.0	–0.1
9a[g][i]	4.79	5.57	5.46	6.92 ($C_6H_3Me_3$) 2.44 ($C_6H_3Me_3$)	7.16 (H_o), 6.86 (H_m, H_p)	[k]	[k]
9b[g][i]	4.79	5.62	5.45	2.52 (C_6Me_6)	6.83 (H_m, H_p)	[k]	[k]
10[g][i]	5.15	6.11		1.93 (Cp*)	[l]	[l]	[l]

[a] Chemical shifts in ppm. [b] Multiplets. [c] Singlets. [d] Broad singlets. [e] In $CDCl_3$. [f] In C_2Cl_4. [g] In $(CD_3)_2CO$. [h] In CD_3NO_2. [i] Detected in a mixture with other products. [j] Difficult to measure owing to instability of **4**. [k] Difficult to measure owing to overlap with signals of other products. [l] Difficult to measure due to overlap with signals of the starting compound **6**.

the nucleophilic degradation[3d,11] by solvent molecules is the first stage of this process. In contrast to **6**, the RhRu complexes **8a**,**b** are stable in refluxing nitromethane.

NMR Spectroscopy

The ^1H and ^{11}B NMR spectroscopic data for complexes **3**–**10** are given in Table 1. For the triple-decker complexes **3**, **4**, **6** and **8** the signals of the borole ring protons are strongly shifted downfield ($\Delta\delta$ = 0.7–1.3 ppm) from the corresponding signals for the sandwich compound **2**. For the arene-type complexes **5**, **7** and **9** these signals are shifted in the same direction but to a lesser extent ($\Delta\delta$ = 0.3–0.4 ppm), thus making ^1H NMR spectroscopy sufficiently informative to distinguish between triple-decker and arene-type structures.

In the ^{11}B NMR spectra of the triple-decker complexes **3**, **6** and **8** the signals of the boron atoms of the borole ligand are shifted upfield ($\Delta\delta$ = 2.8–6.6 ppm) from the corresponding signal for **2**. An analogous shift ($\Delta\delta$ = 2.7–5.0 ppm) was observed earlier for the related cobalt-containing triple-decker complexes [(ring)M(μ-η⁵:η⁵-C_4H_4BR)-CoCp]²⁺ (R = Ph, Cy).[5a,6] For the arene-type complex **5** the signal of the borole ring boron atom is also shifted upfield ($\Delta\delta$ = 6.6 ppm), thus suggesting that ^{11}B NMR spectroscopy is not useful for distinguishing between triple-decker and arene-type structure.

X-ray Diffraction Study

Structure of the Sandwich Complex 2

Complex **2** has the expected sandwich structure (Figure 1). Selected bond lengths and angles are given in Table 2. The planes of the Cp and C_4H_4B cycles are approximately parallel; the dihedral angle Cp/C_4H_4B is equal to 2.42°. The Rh–B [2.304(4) Å] and Rh–C(C_4H_4B) [Rh–C 2.122(4)–2.198(4) Å, av. 2.16 Å] bonds are somewhat shorter than the corresponding bonds in [(η⁵-C_4H_4BPh)-$Rh(PPh_3)_2Cl$] [Rh–B 2.400(5) Å; Rh–C 2.137(4)–2.236(4) Å, av. 2.19 Å].[12] This fact is probably connected to stronger back-donation in the case of **2** as a consequence of the strong electron-donor effect of Cp. An analogous shortening of the Rh–B and Rh–C bonds in [(9-SMe_2-7,8-$C_2B_9H_{10}$)RhCp*]⁺ compared with [(9-SMe_2-7,8-$C_2B_9H_{10}$)Rh(dppe)Cl]⁺ (dppe = $Ph_2PCH_2CH_2PPh_2$) has been reported.[13]

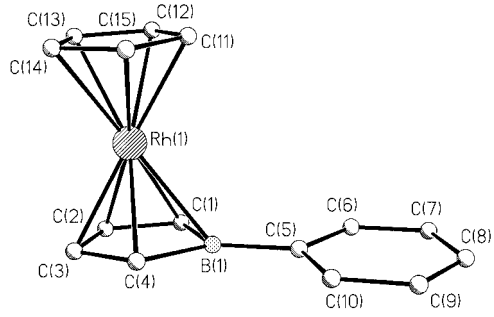

Figure 1. Structure of complex **2**.

Table 2. Selected bond lengths [Å] and angles [°] for complex **2**.

Rh(1)–C(1)	2.198(4)	Rh(1)–C(15)	2.150(5)
Rh(1)–C(2)	2.145(4)	Rh(1)–B(1)	2.304(4)
Rh(1)–C(3)	2.122(4)	C(1)–C(2)	1.425(5)
Rh(1)–C(4)	2.180(4)	C(2)–C(3)	1.445(7)
Rh(1)–C(11)	2.174(4)	C(3)–C(4)	1.418(6)
Rh(1)–C(12)	2.195(4)	B(1)–C(1)	1.543(6)
Rh(1)–C(13)	2.226(4)	B(1)–C(4)	1.547(6)
Rh(1)–C(14)	2.197(5)	B(1)–C(5)	1.562(5)
C(1)–C(2)–C(3)	109.2(4)	C(1)–B(1)–C(4)	101.6(3)
C(2)–C(3)–C(4)	109.9(4)	C(1)–B(1)–C(5)	128.8(4)
C(3)–C(4)–B(1)	109.5(4)	C(4)–B(1)–C(5)	129.5(4)
B(1)–C(1)–C(2)	109.7(4)		

Structures of the Triple-Decker Complexes 6(BF₄)₂ and 8a(BF₄)₂

The structures of complexes **6**$(BF_4)_2$ and **8a**$(BF_4)_2$ contain separated **6** or **8a** cations and BF_4^- anions. The cations

have triple-decker structures formed by three cyclic frameworks, between which two metal atoms are located (Figure 2). Selected bond lengths and angles are given in Tables 3 and 4. In both cases the planes of the cyclic ligands are almost coplanar (dihedral angles Cp*/C_4H_4B = 0.08° and C_4H_4B/Cp = 1.32° for **6**; $C_6H_3Me_3/C_4H_4B$ = 2.39° and C_4H_4B/Cp = 1.36° for **8a**). It was shown earlier that in the case of triple-decker complexes with bridging boratabenzene and pentaphospholyl ligands all bonds in the triple-decker fragment M(ring)M′ are longer than analogous bonds in related mononuclear sandwich compounds.[4b,11] The same pattern, viz. elongation of all bonds in the fragment M(μ-η^5:η^5-C_4H_4BPh)Rh in comparison with the corresponding bonds in **2**, is observed for **6** and **8a**. For example, the B–C [1.593(11) and 1.617(10) Å, av. 1.605 Å] and C–C [1.478(10), 1.506(10), and 1.488(10) Å, av. 1.491 Å)] bonds in the borole ring of **6** are considerably longer than the corresponding bonds in **2** [B–C 1.543(6) and 1.547(6) Å, av. 1.545 Å; C–C 1.425(5), 1.445(7), and 1.418(6) Å, av. 1.429 Å]. Furthermore, the Rh–C(C_4H_4BPh) bonds in **6** [2.174(7)–2.203(8) Å, av. 2.19 Å] and in **8a** [2.182(4)–2.216(4) Å, av. 2.20 Å] are longer than the corresponding bonds in **2** (av. 2.16 Å). This elongation is apparently connected with a loosening of the bonds upon bifacial coordination of the C_4H_4BPh ligand with two metal atoms as compared with its monofacial coordination with only one metal atom. The elongation of the metal-to-ring distances (Δ) in **6** and **8a** in comparison with **2** could be also expected. However, Δ(Rh···C_4H_4BPh) in **6** (1.778 Å) and **8a** (1.795 Å) is not longer, and is even somewhat shorter, than the corresponding distance in **2** (1.792 Å), which may be connected with a compensation of the expected elongation of Δ by shortening of the metal-to-ring distance as a result of the increase of the ring size.

Table 3. Selected bond lengths [Å] and angles [°] for cation **6** (for one of two independent molecules).

Ir(1)–C(1)	2.215(7)	Rh(1)–C(4)	2.174(7)
Ir(1)–C(2)	2.209(7)	Rh(1)–C(11)	2.148(8)
Ir(1)–C(3)	2.208(7)	Rh(1)–C(12)	2.154(8)
Ir(1)–C(4)	2.232(7)	Rh(1)–C(13)	2.164(8)
Ir(1)–C(16)	2.171(8)	Rh(1)–C(14)	2.173(8)
Ir(1)–C(17)	2.168(7)	Rh(1)–C(15)	2.176(8)
Ir(1)–C(18)	2.185(8)	Rh(1)–B(1)	2.289(8)
Ir(1)–C(19)	2.178(7)	C(1)–C(2)	1.478(10)
Ir(1)–C(20)	2.151(8)	C(2)–C(3)	1.506(10)
Ir(1)–B(1)	2.282(9)	C(3)–C(4)	1.488(10)
Rh(1)–C(1)	2.203(8)	B(1)–C(1)	1.593(11)
Rh(1)–C(2)	2.184(7)	B(1)–C(4)	1.617(10)
Rh(1)–C(3)	2.181(7)	B(1)–C(5)	1.541(11)
C(1)–C(2)–C(3)	108.9(6)	C(1)–B(1)–C(4)	99.8(6)
C(2)–C(3)–C(4)	108.4(6)	C(1)–B(1)–C(5)	131.0(6)
C(3)–C(4)–B(1)	111.0(6)	C(4)–B(1)–C(5)	129.2(7)
B(1)–C(1)–C(2)	111.9(6)		

Table 4. Selected bond lengths [Å] and angles [°] for cation **8a**.

Rh(1)–C(1)	2.216(4)	Ru(1)–C(16)	2.204(4)
Rh(1)–C(2)	2.194(4)	Ru(1)–C(17)	2.226(4)
Rh(1)–C(3)	2.182(4)	Ru(1)–C(18)	2.206(4)
Rh(1)–C(4)	2.207(4)	Ru(1)–C(19)	2.233(4)
Rh(1)–C(11)	2.154(4)	Ru(1)–C(20)	2.200(4)
Rh(1)–C(12)	2.161(4)	Ru(1)–C(21)	2.201(4)
Rh(1)–C(13)	2.182(4)	Ru(1)–B(1)	2.279(4)
Rh(1)–C(14)	2.189(4)	C(1)–C(2)	1.470(6)
Rh(1)–C(15)	2.166(4)	C(2)–C(3)	1.491(6)
Rh(1)–B(1)	2.274(5)	C(3)–C(4)	1.468(6)
Ru(1)–C(1)	2.212(4)	B(1)–C(1)	1.596(6)
Ru(1)–C(2)	2.184(4)	B(1)–C(4)	1.600(6)
Ru(1)–C(3)	2.182(4)	B(1)–C(5)	1.552(6)
Ru(1)–C(4)	2.205(4)		
C(1)–C(2)–C(3)	109.2(4)	C(1)–B(1)–C(4)	100.9(3)
C(2)–C(3)–C(4)	109.5(3)	C(1)–B(1)–C(5)	127.7(4)
C(3)–C(4)–B(1)	110.0(3)	C(4)–B(1)–C(5)	131.3(4)
B(1)–C(1)–C(2)	110.3(3)		

Structure of the Arene-Type Complex 5(BF$_4$)$_2$

The structure of complex **5**$(BF_4)_2$ contains separated cation **5** and BF_4^- anions. The cation **5** consists of two sandwich moieties [CpRh(η^5-C_4H_4B)] and [Cp*Rh(η^6-C_6H_5)] connected to each other by a C–B σ-bond (Figure 3). Selected bond lengths and angles are given in Table 5. The planes of the cyclic ligands in each sandwich moiety are almost coplanar (the dihedral angles Cp/C_4H_4B and Cp*/C_6H_5 are equal to 3.52° and 0.47°, respectively). All bonds in the [CpRh(η^5-C_4H_4B)] moiety are very similar in length to the corresponding bonds in **2**, thus indicating that coor-

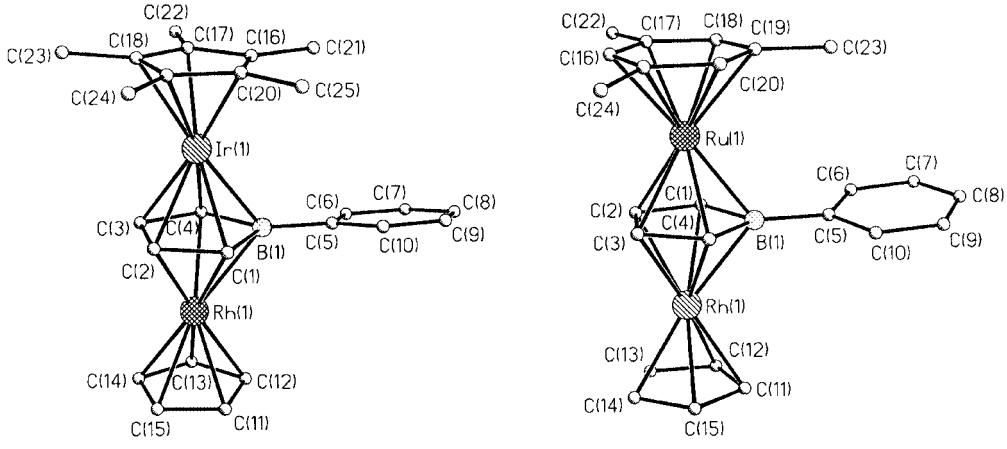

Figure 2. Structures of the triple-decker cations **6** (left) and **8a** (right).

dination of the metal atom at the phenyl substituent of **2** does not lead to serious changes in the sandwich moiety.

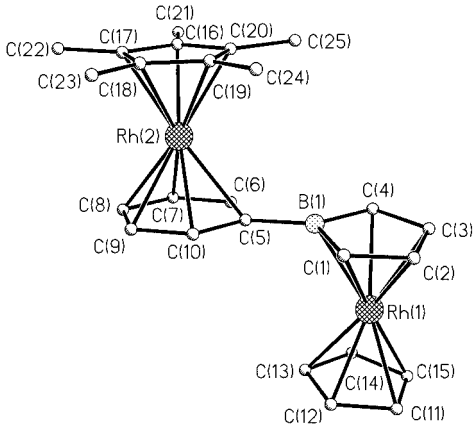

Figure 3. Structure of the arene-type cation **5**.

Table 5. Selected bond lengths [Å] and angles [°] for cation **5**.

Rh(1)–C(1)	2.187(3)	Rh(2)–C(9)	2.259(3)
Rh(1)–C(2)	2.144(3)	Rh(2)–C(10)	2.263(3)
Rh(1)–C(3)	2.159(3)	Rh(2)–C(16)	2.167(3)
Rh(1)–C(4)	2.188(3)	Rh(2)–C(17)	2.169(3)
Rh(1)–C(11)	2.207(4)	Rh(2)–C(18)	2.164(3)
Rh(1)–C(12)	2.188(3)	Rh(2)–C(19)	2.161(3)
Rh(1)–C(13)	2.199(3)	Rh(2)–C(20)	2.171(3)
Rh(1)–C(14)	2.183(3)	C(1)–C(2)	1.422(5)
Rh(1)–C(15)	2.204(3)	C(2)–C(3)	1.441(5)
Rh(1)–B(1)	2.227(4)	C(3)–C(4)	1.432(5)
Rh(2)–C(5)	2.299(3)	B(1)–C(1)	1.533(5)
Rh(2)–C(6)	2.254(3)	B(1)–C(4)	1.545(5)
Rh(2)–C(7)	2.247(3)	B(1)–C(5)	1.561(5)
Rh(2)–C(8)	2.244(3)		
C(1)–C(2)–C(3)	110.1(3)	C(1)–B(1)–C(4)	102.9(3)
C(2)–C(3)–C(4)	109.5(3)	C(1)–B(1)–C(5)	127.5(3)
C(3)–C(4)–B(1)	108.6(3)	C(4)–B(1)–C(5)	129.0(3)
B(1)–C(1)–C(2)	109.0(3)		

Electrochemistry

In principle, the sandwich unit **2** constitutes a poor redox-active component for polynuclear species planned to display intramolecular electronic communication. In fact, in CH_2Cl_2 solution it undergoes an irreversible oxidation at high potential values (controlled potential coulometry consumed 1.5 electrons per molecule, thus indicating that the probable degradation of [**2**]$^+$ leads to redox active by-products). In reality, as we will show, its linking to half-sandwich transition metal units modifies the overall electronic situation such as to improve significantly the electron-transfer ability of the resulting dinuclear species.

As the most representative example, Figure 4 (a) shows the voltammetric picture exhibited by the 30 VE triple-decker CoRh dication [**3**]$^{2+}$.

Two sequential, coulometrically measured one-electron reductions with features of chemical reversibility are displayed, which are interposed by a spurious peak-system, which is assigned to strong adsorption of the reagent.[14] In

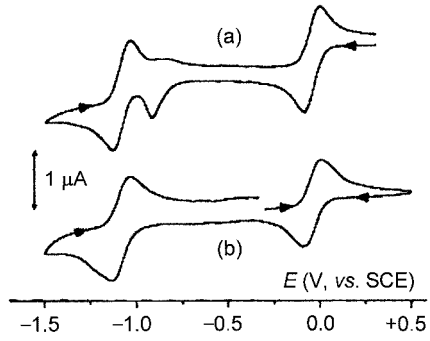

Figure 4. Cyclic voltammetric responses recorded at a platinum electrode in CH_2Cl_2 solution of [**3**]$^{2+}$ (1.0×10^{-3} M): (a) original solution; (b) after exhaustive electrolysis in correspondence of the first reduction. [NBu_4][PF_6] (0.2 M) supporting electrolyte. Scan rate 0.2 V s^{-1}.

fact, as shown in Figure 4 (b), the cyclic voltammetric profile obtained on the exhaustively one-electron-reduced solution (E_w = –0.5 V) no longer exhibits such an anomalous process. More importantly, it can be seen that the response after exhaustive electrolysis is quite complementary to the original one, thus confirming the stability of the corresponding monocation [**3**]$^+$ not only over the short timescale of cyclic voltammetry, but also over the longer time of macroelectrolysis. No traces of oxidation of the parent subunit **2** were detected.

As a matter of fact, analysis of the cyclic voltammograms relevant to the first reduction (due to the above-cited absorption phenomena, mechanical cleaning of the electrode was needed after each scan) with a scan rate varying from 0.02 V s^{-1} to 1.00 V s^{-1} agrees with the occurrence of a simple, chemically and electrochemically reversible, one-electron reduction. In fact: (i) the current ratio i_{pa}/i_{pc} is constantly equal to unity; (ii) the current function $i_{pc} \cdot v^{-1/2}$ is substantially constant; and (iii) the peak-to-peak separation approaches the theoretical value of 59 mV. It should be noted that the electrochemical reversibility indicates that the monocation substantially maintains the geometry of the dication precursor.[14]

In reality, among the dinuclear complexes studied here, the appearance of two consecutive one-electron reductions is essentially limited to [**3**]$^{2+}$, as the other dications (except for [**8a**]$^{2+}$) only display a one-electron reduction, the extent of chemical reversibility of which varies with the nature of the different half-sandwich subunit. As a matter of fact, the i_{pa}/i_{pc} current ratio for the pertinent reduction process is lower than unity in all cases at low scan rate and progressively tends to unity at high scan rates.

Table 6 compiles the formal electrode potentials of the above-cited redox changes, together with the lifetime ($t_{1/2}$) of the different monocations, which, because of the substantial invariance of the responses with concentration, have been assumed to be coupled to a first-order chemical complication.[14]

Apart from the expected roles of the inductive effects of the half-sandwich units added to **2** upon the electrode potentials, the higher stability of the triple-decker mono-

Table 6. Formal electrode potentials (V, vs. SCE), peak-to-peak separations [mV], current ratios and lifetimes [s] for the electrogenerated products of the redox changes exhibited by the complexes under study in CH_2Cl_2 solution.

Complex	E_p[a][b]	$E°'_{2+/+}$	ΔE_p[b]	i_{pa}/i_{pc}[c]	$t_{1/2\ (monocation)}$	$E°'_{+/0}$	ΔE_p[b]	i_{pa}/i_{pc}[c]
2	+1.12							
$[\mathbf{3}]^{2+}$		–0.04	70	1	stable	–1.08	90	1
$[\mathbf{6}]^{2+}$		–0.31	66	0.7	12			
$[\mathbf{8a}]^{2+}$		–0.26	71	0.8	26	–1.06[a][b]		
$[\mathbf{5}]^{2+}$	+1.65[d]	–0.55	62	0.4[e]	0.06			

[a] Peak-potential value for irreversible processes. [b] Measured at 0.2 V s^{-1}. [c] Measured at 0.05 V s^{-1}. [d] Two-electron process. [e] Measured at 1.0 V s^{-1}.

cations with respect to the extreme lability of the arene-type monocation $[\mathbf{5}]^+$ deserves attention.

Spectroelectrochemistry of the $[3]^{2+}/[3]^+$ Redox Change

UV/Vis spectroelectrochemical measurements on the one-electron reduction of the dication $[\mathbf{3}]^{2+}$ were performed in CH_2Cl_2 solution at 298 K using an OTTLE cell. As Figure 5 shows, the original red dication displays a prominent band at λ_{max} = 320 nm together with a few less-intense transitions at 265, 449 and 520 nm. Upon reduction, the intensity of such bands progressively decreases, except for the transition at 265 nm, which progressively increases with a concomitant blue-shift to 244 nm.

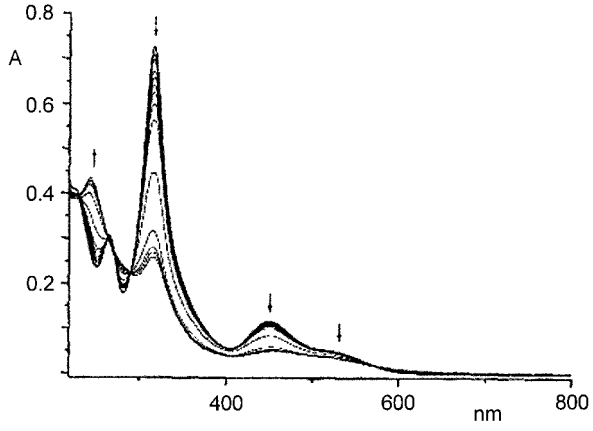

Figure 5. UV/Vis spectra recorded in CH_2Cl_2 solution of $[\mathbf{3}]^{2+}$ (1.0×10^{-3} M) upon one-electron reduction in an OTTLE cell. $[NBu_4][PF_6]$ (0.2 M) supporting electrolyte. E_w = –0.1 V vs. Ag pseudoreference electrode.

The appearance of four isosbestic points, which are due to the mixture of $[\mathbf{3}]^{2+}/[\mathbf{3}]^+$, further supports the chemical reversibility of the electron transfer.

In order to test for a possible assignment of the two lowest energy bands of $[\mathbf{3}]^{2+}$ as metal-to-metal charge transfer (MMCT) absorptions, their solvent dependence concerned with both position and band width was checked. Figure 6 shows the pertinent spectra in tetrahydrofuran, dichloromethane and acetonitrile. In spite of the small blue-shift observed on going from CH_2Cl_2 to the better donor solvents THF and MeCN, the measured half-height band width, $\Delta\nu_{1/2(exp)}$, is too small with respect to the theoretical one, which for a Class II mixed-valent complex is expected to be: $\Delta\nu_{1/2} = [2310(\nu_{max} - \Delta E°)]^{1/2}$, where $\Delta E°$ is the separation of potentials (in cm^{-1}) for the formal redox couples in non-interacting $[CpRh(\eta^5\text{-}C_4H_4BPh)]$ (complex **2**) and $[Cp^*Co(\eta^5\text{-}C_4H_4BPh)]$.[15] In fact, assuming that a MMCT for $[\mathbf{3}]^{2+}$ would involve a Co^{III}-Rh^{III} to Co^{II}-Rh^{IV} transition, a value of $\Delta E°$ = 1.15 V (= 9275 cm^{-1}) may be used, taking into account the $E°'$ measured for the Rh^{III}/Rh^{IV} redox change in $[\mathbf{2}]^+$ (+1.12 V) and approximating the $E°$ of the Co^{II}/Co^{III} redox change in $[Cp^*Co(\eta^5\text{-}C_4H_4BPh)]$ to the formal electrode potential of the first reduction of $[\mathbf{3}]^{2+}$ ($E°'$ = –0.03 V). Accordingly, we obtain $\Delta\nu_{1/2(calc)}$ = 4860 cm^{-1} and $\Delta\nu_{1/2(calc)}$ = 5492 cm^{-1} for the two lowest energy bands in dichloromethane, which is almost two times

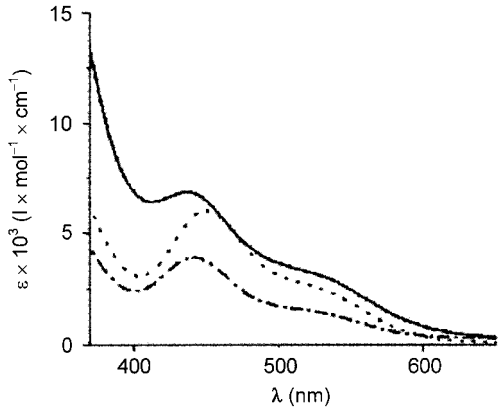

Figure 6. Comparison of the optical spectra of $[\mathbf{3}]^{2+}$ in: MeCN (–), CH_2Cl_2 (·····), THF (·–·–·).

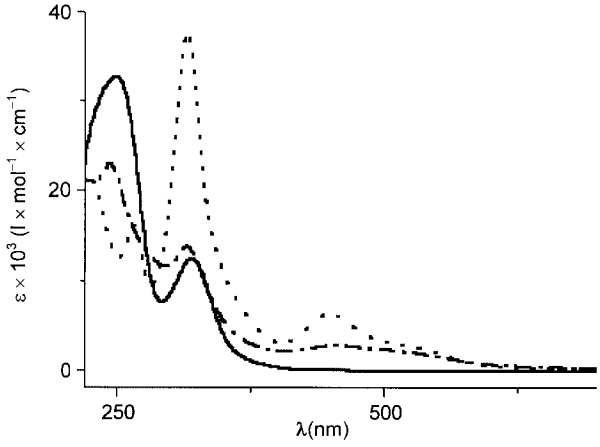

Figure 7. Comparative optical spectra of: (a) **2** (1.4×10^{-3} M)(); (b) $[\mathbf{3}]^{2+}$ (1.0×10^{-3} M) (·····); (c) $[\mathbf{3}]^+$ (1.0×10^{-3} M) (·–·–·). CH_2Cl_2 solution.

greater than the experimental values $\Delta\nu_{1/2(exp)}$ = 2862 cm^{-1} and $\Delta\nu_{1/2(exp)}$ = 2852 cm^{-1}, respectively. This result therefore rules out the MMCT assignment.

Comparison of the UV/Vis spectra of the triple-deckers [**3**]$^{2+}$ and [**3**]$^{+}$ with the subunit **2** (Figure 7) suggests that the MLCT absorptions at 320 and 244 nm are substantially contributed by the rhodium subunit, whereas the d-d transitions of the Co^{III}/Co^{II} centres in [**3**]$^{2+/+}$ could be responsible for the absorptions at wavelengths higher than 400 nm.

EPR Measurements of the Electrogenerated Monocation [3]$^{+}$

Figure 8 shows the low-temperature X-band EPR spectrum of the electrogenerated 31 VE triple-decker monocation [**3**]$^{+}$ in CH_2Cl_2 solution.

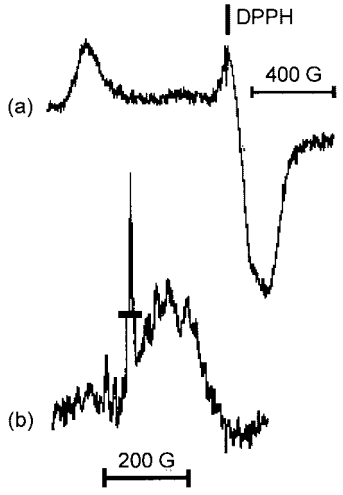

Figure 8. X-band EPR spectrum of [**3**]$^{+}$ in CH_2Cl_2 solution. T = 100 K: (a) first derivative; (b) second derivative.

The broad spectrum shown in Figure 8 (see part a; peak-to-peak separation ca. 1050(5) G) exhibits three rhombic signals with g_i values [g_l = 2.497(8); g_m = 1.971(8); g_h = 1.899(8); $<g>$ = 1/3(g_l + g_m + g_h) = 2.122(8), with l, m and h standing for low-, medium- and high-field, respectively] that are very different from that of a single unpaired electron ($g_{electron}$ = 2.0023). In the second derivative mode, the two partially overlapped high-field signals display resolution of the underlying hpf signals.

A lineshape analysis can be carried out taking into account the anisotropic S = 1/2 Electron Spin Hamiltonian (Zeeman interaction) with resolution of the metallic hyperfine (hpf) signals (IAS interaction).[16]

The second derivative mode is crucial for the understanding of the nature of the metal ion directly involved in the anisotropic IAS interaction. In fact, as shown in Figure 8(see part b), in the high-field region it displays a structured hpf multiplet constituted by almost six well-separated signals of equal intensity [1:1:1:1:1:1; $a_{m,l}$ = 48(8) G], which testifies to the direct coupling of the S = 1/2 unpaired electron with the magnetically active ^{59}Co nucleus [I(^{59}Co) = 7/2; natural abundance = 100%]. The theoretically expected octuplet typical of low-spin Co^{II} centres is not completely resolved as a consequence of both the actual anisotropic linewidth, which affects the overall signals, and the active A-strain effects, which narrow the eight hpf signals to different degrees.[16] The lineshape analysis rules out the assignment of the present high field multiplet to the Rh^{II} subunit in that the expected anisotropic signals should exhibit poorly resolved doublets [I(^{103}Rh) = 1/2; natural abundance = 100%] and the corresponding g_i signals would resonate at different field values.[17]

Moreover, no attribution of the detected multiplet to magnetically coupled ligand ^{1}H nuclei can be proposed as the actual number and the relative intensities of such signals are totally in contrast with the present spectral resolution.

The simulated geometry and the pertinent MO diagram distribution displayed in Figure 9 below confirm the above analysis. In fact, the SOMO of the electrogenerated monocation is mainly constituted by the 3d Co^{II} AOs, with a very minor contribution arising from the Rh^{III} centre and the H and C of the aromatic ligands. On this basis, the intense and narrow signal overlapping the second derivative multiplet is probably due to an organic radical by-product.

Raising the temperature to the glassy-fluid transition (T = 178 K) the large axial spectrum collapses into a broad and unresolved isotropic signal. The lack of Co^{II} hpf resolution in fluid solution is not surprising considering the large Co^{II} λ spin-orbit coupling constant and possible structural anisotropies which fasten the electron spin relaxation rates.[16,18]

At room temperature the spectrum exhibits features compatible with those recorded under glassy conditions [g_{iso} = 2.02(8) and ΔH_{iso} = 470(8) G], although no hpf splittings are detected [likely due to the actual linewidth, (ΔH_{iso}/7 = 67(8) G) $\geq$ a_{iso}(Co)]. These findings suggest that the primary geometry of the monocation is maintained under different experimental conditions. Upon fast refreezing, the previous rhombic signal is partially recovered as a consequence of some chemical lability under not perfectly inert atmosphere.

Molecular Orbital Calculations for [3]$^{2+}$

In order to support the interpretation of the EPR spectrum of the 31 VE triple-decker cation [**3**]$^{+}$, an extended Hückel analysis was carried out. Fragment analyses were performed for a model built by using bond distances and angles taken as the average of the experimental values in analogous complexes.[19] It has been shown previously that the extended Hückel method combined with INDO calculations gives reliable results for μ-borole triple-decker complexes.[20]

This model, and fragments thereof, together with the reference system, are shown at the bottom of Figure 9, which depicts the interaction between the orbitals of the [Cp*Co]$^{2+}$ (shown on the right) and [CpRh(η^5-C_4H_4BPh)] (shown on the left) fragments that generate the [CpRh(μ-η^5:η^5-C_4H_4BPh)CoCp*]$^{2+}$ triple-decker.

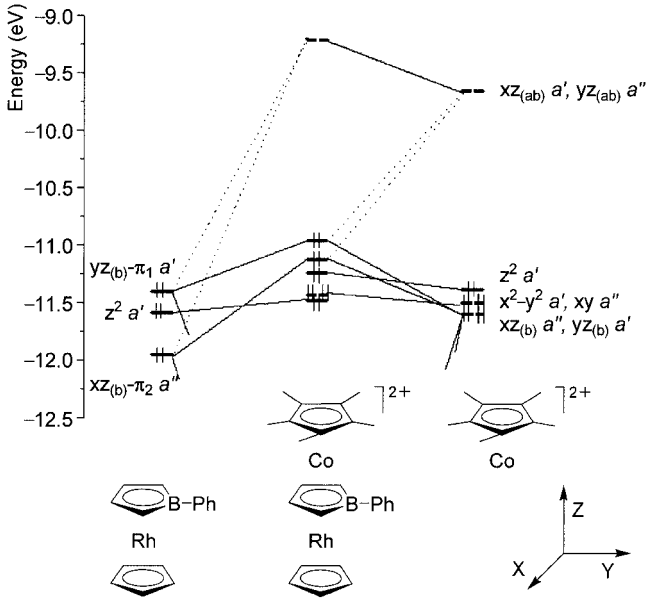

Figure 9. FMO interaction between the frontier orbitals of the $[Cp^*Co]^{2+}$ and $[CpRh(\eta^5\text{-}C_4H_4BPh)]$ fragments to give the $[CpRh(\mu\text{-}\eta^5\text{:}\eta^5\text{-}C_4H_4BPh)CoCp^*]^{2+}$ triple-decker.

The symmetry labels used are those of the C_s point group, which is the lowest symmetry exhibited by the triple-decker model or fragments discussed here, and is imposed by $[CpRh(\mu\text{-}\eta^5\text{:}\eta^5\text{-}C_4H_4BPh)CoCp^*]^{2+}$. The frontier orbital region is characterized by two orthogonal three-orbital-four-electron systems. Indeed, the bonding and antibonding combinations Cp*(π)-Co(d_{xz}) and Cp*(π)-Co(d_{yz}) spawn two degenerate couples of orbitals both having the right a′ and a″ symmetry and the appropriate fit in energy to interact with the bonding set of orbitals Cp(π)-Rh(d_{xz})-C_4H_4BPh(π) and Cp(π)-Rh(d_{yz})-C_4H_4BPh(π). The repulsive interaction between two filled sets of orbitals, which gives rise to the antibonding HOMO and HOMO–1, is therefore stabilised by the interaction with the empty antibonding Cp*(π)-Co(d_{xz}) and Cp*(π)-Co(d_{yz}) orbitals. As a consequence of this interaction, two almost degenerate LUMOs are present, which are antibonding combinations of the fragments $[CpRh(\eta^5\text{-}C_4H_4BPh)]$ and CoCp*, with 33% contribution of Co(d_{xz}) or Co(d_{yz}) and only 4% of Rh(d_{xz}) or Rh(d_{yz}). One of these orbitals is shown in Figure 9, where the major contribution of the cobalt-containing half is evident.

According to these findings, both reduction processes of the 30 VE cation $[\mathbf{3}]^{2+}$ involve mainly the cobalt atom. This is in agreement with the EPR analysis, which also supports a predominant contribution of cobalt in the SOMO of the 31 VE cation $[\mathbf{3}]^{+}$. The absence of oxidation processes for $[\mathbf{3}]^{2+}$ in the experimental window, which is in contrast with the higher energy of its HOMO with respect to **2**, may be explained by the positive charge of this complex, which, on an electrostatic basis, would inhibit any further electron removal.

Conclusions

The electrophilic attack of dicationic fragments $[(ring)M]^{2+}$ has been shown to proceed mainly at the borole ring of the *B*-phenylborole complex **2** to give 30 VE triple-decker complexes $[CpRh(\mu\text{-}\eta^5\text{:}\eta^5\text{-}C_4H_4BPh)M(ring)]^{2+}$. These complexes are stable when (ring)M is Cp*Co, Cp*Ir and (arene)Ru. However, the Cp*Rh analogue **4** transforms into the arene-type complex **5** at room temperature. Comparison of X-ray structural data for complexes **2**, **5**, **6** and **8a** reveals that the coordination of $[(ring)M]^{2+}$ species to the borole ring of **2** leads to elongation of the bonds within this ring, whereas the coordination to the benzene ring does not cause significant changes in the bonds within the borole ring.

The electrochemical data demonstrate the much higher stability of the 31 VE triple-decker monocations $[\mathbf{3}]^{+}$, $[\mathbf{6}]^{+}$ and $[\mathbf{8a}]^{+}$ (formed by one-electron reduction of the corresponding dications) compared with the 31 VE arene-type monocation $[\mathbf{5}]^{+}$. For instance, $[\mathbf{3}]^{+}$ is stable not only over the short times of cyclic voltammetry, but also over the long times of macroelectrolysis. UV/Vis and EPR spectral measurements as well as MO calculations suggest that the reduction process $[\mathbf{3}]^{2+}/[\mathbf{3}]^{+}$ involves mainly the cobalt atom.

Experimental Section

General: The reactions were carried out under an inert atmosphere in dry solvents. The isolation of products was conducted in air. Starting materials **2**,[21] $[Cp^*CoCl_2]_2$,[22] $[Cp^*RhCl_2]_2$,[23] $[Cp^*IrCl_2]_2$,[23] $[(\eta^6\text{-}C_6H_3Me_3\text{-}1,3,5)RuCl_2]_2$[24] and $[(\eta^6\text{-}C_6Me_6)RuCl_2]_2$[25] were prepared as described in the literature. ^1H and $^{11}B\{^1H\}$ NMR spectra were recorded on a Bruker AMX-400 spectrometer (^1H: 400.13; ^{11}B: 128.38 MHz) relative to the residual protons of the solvents (^1H) or $BF_3{\cdot}Et_2O$ (^{11}B, external standard). Materials and apparatus for electrochemistry and joint EPR spectroscopy have been described elsewhere.[26] Unless otherwise specified, potential values are referred to the Saturated Calomel Electrode (SCE). Under the present experimental conditions, the one-electron oxidation of ferrocene occurs at $E^{\circ\prime}$ = +0.39 V. The UV/Vis spectroelectrochemical measurements were carried out using a Perkin–Elmer Lambda 900 UV/Vis spectrophotometer and an OTTLE (optically transparent thin-layer electrode) cell[27] equipped with a Pt minigrid working electrode (32 wires/cm), a Pt minigrid auxiliary electrode, an Ag wire pseudoreference and CaF_2 windows. The electrode potential was controlled during electrolysis by an Amel potentiostat 2059 equipped with an Amel function generator 568. Nitrogen-saturated solutions of the compound under study were used with $[NBu_4][PF_6]$ (0.2 M) as supporting electrolyte. The working potential was fixed at the peak potential of the process under study and the spectra were collected stepwise after each 2 min electrolysis. Extended Hückel calculations were performed using the CACAO98 for Windows programs package.[28] Bond distances and angles of the model molecule were taken as the average of the experimental values. Slater orbital ionization energies were corrected from the default ones by taking H_{ii} from a set of values calculated by DFT theory.[29] The exponentials of the Slater orbitals were taken from the program library.

Synthesis of $3(BF_4)_2$: A mixture of $[Cp^*CoCl_2]_2$ (43 mg, 0.08 mmol) and $AgBF_4{\cdot}3$ dioxane (150 mg, 0.33 mmol) in $MeNO_2$ (1 mL) was

stirred for 0.5 h at room temperature. The precipitate of AgCl was centrifuged off and the solution obtained was added to **2** (50 mg, 0.16 mmol). The reaction mixture was stirred for 2 h. Diethyl ether (ca. 10 mL) was then added to precipitate **3**$(BF_4)_2$ as a red solid, which was reprecipitated twice from nitromethane by addition of diethyl ether. Yield 50 mg (46%). $C_{25}H_{29}B_3CoF_8Rh$ (675.76): calcd. C 44.44, H 4.33; found C 44.37, H 4.25.

Synthesis of 5$(BF_4)_2$: A mixture of $[Cp^*RhCl_2]_2$ (40 mg, 0.06 mmol) and $AgBF_4$·3 dioxane (120 mg, 0.26 mmol) in $MeNO_2$ or Me_2CO (1 mL) was stirred for 0.5 h at room temperature. The precipitate of AgCl was centrifuged off and the solution obtained was added to **2** (40 mg, 0.13 mmol). The reaction mixture was stirred for 2 h. Diethyl ether (ca. 10 mL) was then added to precipitate **5**$(BF_4)_2$ as a yellow solid, which was reprecipitated twice from acetone by addition of diethyl ether. Yield 65 mg (70%). $C_{25}H_{29}B_3F_8Rh_2$ (719.72): calcd. C 41.72, H 4.06; found C 41.44, H 4.09.

Synthesis of 6$(BF_4)_2$ and 8a,b$(BF_4)_2$: Me_2CO (1 mL) was added to a mixture of $[(ring)MCl_2]_2$ [(ring)M = Cp*Ir, (η^6-$C_6H_3Me_3$-1,3,5)Ru, and (η^6-C_6Me_6)Ru] (0.08 mmol) and $AgBF_4$·3 dioxane (150 mg, 0.33 mmol). The reaction mixture was stirred for ca. 0.5 h and the precipitate of AgCl was centrifuged off. The solution obtained was added to **2** (50 mg, 0.16 mmol) and stirred for 2 h at –15 °C. After warming to room temperature, diethyl ether (ca. 10 mL) was added to precipitate a bright-coloured solid, which was reprecipitated twice from acetone by addition of diethyl ether.

6$(BF_4)_2$: Yellow, yield 84 mg (64%). $C_{25}H_{29}B_3F_8IrRh$ (809.05): calcd. C 37.11, H 3.61; found C 37.05, H 3.67.

8a$(BF_4)_2$: Orange, yield 84 mg (74%). $C_{24}H_{26}B_3F_8RhRu$ (702.86): calcd. C 41.01, H 3.73; found C 40.46, H 3.61.

8b$(BF_4)_2$: Orange, yield 80 mg (67%). $C_{27}H_{32}B_3F_8RhRu$ (744.94): calcd. C 43.53, H 4.33; found C 43.17, H 4.65.

X-ray Crystallographic Study: Crystals of **2** were grown by slow evaporation of its petroleum ether solution. Crystals of **5**$(BF_4)_2$, **6**$(BF_4)_2$ and **8a**$(BF_4)_2$ were obtained by slow interdiffusion of a two-phase system containing diethyl ether and an acetone solution of the complex. The principal crystallographic data, procedures for collecting experimental data, and characteristics of structure refinement are listed in Table 7. Single-crystal X-ray diffraction experiment for **2** was carried out with a Syntex $P2_1$ diffractometer (graphite monochromated Mo-K_α radiation, $\theta/2\theta$ scans technique) at 153 K. Analogous experiments for **5**$(BF_4)_2$, **6**$(BF_4)_2$ and **8a**$(BF_4)_2$ were carried out with a Bruker SMART 1000 CCD area detector, with graphite-monochromated Mo-K_α radiation (λ = 0.71073 Å, ω-

Table 7. Crystal data and structure-refinement parameters for **2**, **5**, **6** and **8a**.

	2	**5**$(BF_4)_2$	**6**$(BF_4)_2$	**8a**$(BF_4)_2$
Empirical formula	$C_{15}H_{14}BRh$	$C_{25}H_{29}B_3F_8Rh_2$	$C_{25}H_{25}B_3F_8IrRh$	$C_{24}H_{26}B_3F_8RhRu$
Formula mass	307.98	719.73	804.99	702.86
Crystal colour, habit	colourless needle	colourless needle	orange plate	red needle
Crystal size [mm]	0.55 × 0.30 × 0.25	0.50 × 0.30 × 0.15	0.45 × 0.20 × 0.05	0.50 × 0.30 × 0.15
Crystal system	orthorhombic	monoclinic	monoclinic	triclinic
Space group	$P2_12_12_1$	$P2_1/n$	$P2_1/c$	$P\bar{1}$
a [Å]	5.927(2)	12.467(4)	16.795(7)	8.716(2)
b [Å]	12.632(4)	10.216(3)	17.947(8)	11.944(3)
c [Å]	16.352(4)	20.841(6)	18.267(8)	13.392(3)
α [°]	90	90	90	92.633(5)
β [°]	90	96.083(6)	91.945(9)	97.688(5)
γ [°]	90	90	90	107.719(4)
V [Å^3]	1224.3(7)	2639.3(12)	5503(4)	1310.7(5)
Z	4	4	8	2
D(calcd.) [g cm^{-3}]	1.671	1.811	1.943	1.781
Diffractometer	Syntex $P2_1$	Bruker SMART 1000 CCD		
Temperature [K]	153	140	120	110
Radiation	Mo-K_α (λ = 0.71073)			
Scan mode	θ–2θ	φ and ω		
$2\theta_{max}$ [°]	60.12	60.12	54.20	56.70
Abs.coeff. μ(Mo-*K*a) [cm^{-1}]	13.65	13.21	54.99	12.75
Absorption correction	multi-scan			
$T_{max.}$ and $T_{min.}$		0.862 and 0.520	0.155 and 0.048	0.928 and 0.594
Completeness [%]	99.1	99.4	99.7	98.9
Structure solution	direct methods			
Refinement method	full-matrix least-squares on F^2			
Collected reflections	2112	21 609	52 556	14 197
Independent reflections	2069 (R_{int} = 0.0190)	7703 (R_{int} = 0.0314)	12 110 (R_{int} = 0.0716)	6692 (R_{int} = 0.0287)
Observed reflections [$I > 2\sigma(I)$]	2024	6258	7994	5305
Abs. structure parameter	–0.05(6)			
Parameters	154	343	685	334
R_1 (on *F* for obsd. reflections)	0.0332	0.0528	0.0442	0.0511
wR_2 (on F^2 for all reflections)	0.0998	0.1333	0.1166	0.1370
Weighting scheme	$w^{-1} = \sigma^2(F_o^2) + (aP)^2 + bP$, $P = 1/3(F_o^2 + 2F_c^2)$			
a	0.1000	0.1000	0.0607	0.0755
b				2.8474
F(000)	616	1424	3072	695
GOOF	0.940	1.038	0.996	1.082
Largest diff. peak and hole [e Å^{-3}]	1.779 and –0.816	5.915 and –1.271	3.369 and –1.811	3.364 and –1.040

scans with 0.3° steps in ω and 10 s per frame exposure) at 110–140 K. The low temperature of the crystals was maintained with a Cryostream (Oxford Cryosystems) open-flow N_2 gas cryostat. Reflection intensities were integrated by using the SAINT software[30] and the semi-empirical method SADABS.[31] The structures were solved by direct methods and refined by full-matrix least-squares against F^2_{hkl} in an anisotropic (for non-hydrogen atoms) approximation. All hydrogen atoms in the structures were placed in geometrically calculated positions and included in the final refinement using the "riding" model with $U_{iso}(H)$ parameters equal to 1.2 $U_{eq}(C_i)$ or 1.5 $U_{eq}(C_{ii})$, where $U(C_i)$ and $U(C_{ii})$ are the equivalent thermal parameters of the methyne and methyl carbon atoms, respectively, to which the corresponding H atoms are bonded. All calculations were performed on an IBM PC/AT using the SHELXTL software.[32]

CCDC-238739 (for **2**), -238740 [for **5**$(BF_4)_2$], -238741 [for **6**$(BF_4)_2$] and -238742 [for **8a**$(BF_4)_2$] contain the supplementary crystallographic data for this paper. These data can be obtained free of charge from The Cambridge Crystallographic Data Centre via www.ccdc.cam.ac.uk/data_request/cif.

Acknowledgments

This work was supported by the Russian Foundation for Basic Research (Grant No. 03-03-32214), as well as the General Chemistry and Material Science Division of RAS (Grant No 05-07). P. Z. gratefully acknowledges financial support from the Università di Siena (PAR, 2003).

[1] a) C. White, S. J. Thompson, P. M. Maitlis, *J. Chem. Soc., Dalton Trans.* **1977**, 1654–1661 (*Rh and Ir*); b) M. A. Bennett, T. W. Matheson, *J. Organomet. Chem.* **1979**, *175*, 87–93 (*Ru*); c) S. L. Grundy, P. M. Maitlis, *J. Organomet. Chem.* **1984**, *272*, 265–282 (*Ir*); d) D. A. Herebian, C. S. Schmidt, W. S. Sheldrick, C. van Wüllen, *Eur. J. Inorg. Chem.* **1998**, 1991–1998 (*Rh and Ir*); e) C. M. Alvarez, R. J. Angelici, A. Sygula, R. Sygula, P. W. Rabideau, *Organometallics* **2003**, *22*, 624–626 (*Ir*).

[2] A. R. Kudinov, M. I. Rybinskaya, *Izv. Akad. Nauk, Ser. Khim.* **1999**, 1636–1642 [*Russ. Chem. Bull.* **1999**, *48*, 1615–1621 (Engl. Transl.)].

[3] a) H. Werner, A. Salzer, *Synth. Inorg. Met.-Org. Chem.* **1972**, *2*, 239–248; b) A. Salzer, H. Werner, *Angew. Chem. Int. Ed. Engl.* **1972**, *11*, 930–932; c) A. R. Kudinov, M. I. Rybinskaya, Yu. T. Struchkov, A. I. Yanovskii, P. V. Petrovskii, *J. Organomet. Chem.* **1987**, *336*, 187–197; d) G. E. Herberich, U. Englert, F. Marken, P. Hofmann, *Organometallics* **1993**, *12*, 4039–4045; e) G. E. Herberich, U. J. Jansen, *Organometallics* **1995**, *14*, 834–841; f) A. R. Kudinov, A. A. Fil'chikov, P. V. Petrovskii, M. I. Rybinskaya, *Izv. Akad. Nauk, Ser. Khim.* **1999**, 1364–1367 [*Russ. Chem. Bull.* **1999**, *48*, 1352–1355 (Engl. Transl.)].

[4] a) G. E. Herberich, U. Englert, D. Pubanz, *J. Organomet. Chem.* **1993**, *459*, 1–9; b) G. E. Herberich, U. Englert, B. Ganter, C. Lamertz, *Organometallics* **1996**, *15*, 5236–5241; c) A. R. Kudinov, D. A. Loginov, Z. A. Starikova, P. V. Petrovskii, *J. Organomet. Chem.* **2002**, *649*, 136–140.

[5] a) G. E. Herberich, B. J. Dunne, B. Hessner, *Angew. Chem. Int. Ed. Engl.* **1989**, *28*, 737–738; b) G. E. Herberich, U. Büschges, B. A. Dunne, B. Hessner, N. Klaff, D. P. J. Köffer, K. Peters, *J. Organomet. Chem.* **1989**, *372*, 53–60.

[6] A. R. Kudinov, D. A. Loginov, D. V. Muratov, P. V. Petrovskii, *Izv. Akad. Nauk, Ser. Khim.* **2001**, 1267–1268 [*Russ. Chem. Bull.* **2001**, *50*, 1332–1333 (Engl. Transl.)].

[7] All the dicationic fragments were generated as labile solvates $[(ring)M(Solv)_3]^{2+}$ (Solv = $MeNO_2$, Me_2CO) by treatment of $[(ring)MCl_2]_2$ with $AgBF_4$.

[8] All the cationic complexes described here were isolated as salts with the BF_4^- anion (the anions are omitted in the schemes).

[9] G. Fairhurst, C. White, *J. Chem. Soc., Dalton Trans.* **1979**, 1531–1538.

[10] Symmetrization of the FeMn complex [CpFe(μ-η^5:η^5-C_4H_4BPh)Mn$(CO)_3$] has been shown to give a mixture of [CpFe(μ-η^5:η^5-C_4H_4BPh)FeCp] and [$(CO)_3$Mn(μ-η^5:η^5-C_4H_4BPh)Mn$(CO)_3$]: G. E. Herberich, D. P. J. Köffer, K. M. Peters, *Chem. Ber.* **1991**, *124*, 1947–1952.

[11] A. R. Kudinov, D. A. Loginov, Z. A. Starikova, P. V. Petrovskii, M. Corsini, P. Zanello, *Eur. J. Inorg. Chem.* **2002**, 3018–3027, and references cited therein.

[12] G. E. Herberich, W. Boveleth, B. Hessner, M. Hostalek, D. P. J. Köffer, M. Negele, *J. Organomet. Chem.* **1987**, *319*, 311–326.

[13] A. R. Kudinov, D. S. Perekalin, P. V. Petrovskii, K. A. Lyssenko, G. V. Grintselev-Knyazev, Z. A. Starikova, *J. Organomet. Chem.* **2002**, *657*, 115–122.

[14] P. Zanello, *Inorganic Electrochemistry. Theory, Practice and Application*, RS·C, Cambridge, UK, **2003**.

[15] N. Dowling, P. M. Henry, N. A. Lewis, H. Taube, *Inorg. Chem.* **1981**, *20*, 2345–2348.

[16] F. E. Mabbs, D. Collison, *Electron Paramagnetic Resonance of d Transition Metal Complexes*, in *Studies in Inorganic Chemistry*, Vol. 16, Elsevier, New York, **1992**.

[17] a) C. Bianchini, M. Peruzzini, F. Laschi, P. Zanello, *Synthesis Characterization and Chemistry of Rhodium(II) Organometallic Complexes Stabilized by Tripodal Polyphosphine Ligands*, in *Topics in Physical Organometallic Chemistry* (Ed.: M. F. Gielen), Freund Publ. House Ltd, U.K, **1992**, vol. 4, 139–219; b) J. E. Collins, M. P. Castellani, A. L. Rheingold, E. J. Miller, W. E. Geiger, A. L. Rieger, P. H. Rieger, *Organometallics* **1995**, *14*, 1232–1238.

[18] A. Bencini, D. Gatteschi, *ESR Spectra of Metal Complexes of the First Transition Series in Low-Symmetry Environments*, in *Transition Metal Chemistry*, Vol. 8, M. Dekker, New York, **1982**.

[19] The Cambridge Structural Database: version 5.25, November 2003 and VISTA 2.0.

[20] R. Gleiter, I. Hyla-Kryspin, G. E. Herberich, *J. Organomet. Chem.* **1994**, *478*, 95–102.

[21] G. E. Herberich, U. Büschges, B. Hessner, H. Lüthe, *J. Organomet. Chem.* **1986**, *312*, 13–25.

[22] M. J. Macazaga, S. Delgado, R. M. Medina, J. R. Masaguer, *J. Organomet. Chem.* **1984**, *277*, 423–426.

[23] C. White, A. Yates, P. M. Maitlis, *Inorg. Synth.* **1992**, *29*, 228–234.

[24] M. A. Bennett, A. K. Smith, *J. Chem. Soc., Dalton Trans.* **1974**, 233–241.

[25] M. A. Bennett, T.-N. Huang, T. W. Matheson, A. K. Smith, *Inorg. Synth.* **1982**, *21*, 74–78.

[26] P. Zanello, F. Laschi, M. Fontani, C. Mealli, A. Ienco, K. Tang, X. Jin, L. Li, *J. Chem. Soc., Dalton Trans.* **1999**, 965–970.

[27] M. Krejčik, M. Daněk, F. Hartl, *J. Electroanal. Chem.* **1991**, *317*, 179–187.

[28] C. Mealli, D. M. Proserpio, *J. Chem. Educ.* **1990**, *67*, 399.

[29] A. Vela, J. L. Gázquez, *J. Phys. Chem.* **1988**, *92*, 5688–5693.

[30] SMART v. 5.051 and SAINT v. 5.00, Area detector control and integration software, **1998**, Bruker AXS Inc., Madison, WI-53719, USA.

[31] G. M. Sheldrick, *SADABS*, **1997**, Bruker AXS Inc., Madison, WI-53719, USA.

[32] G. M. Sheldrick, *SHELXTL-97*, v. 5.10, Bruker AXS Inc., Madison, WI-53719, USA.

Received: October 27, 2004

